

Quantifying Chromosome Structural Reorganizations during Differentiation, Reprogramming, and Transdifferentiation

Xiakun Chu^{1,3} and Jin Wang^{2,3,*}

¹Advanced Materials Thrust, The Hong Kong University of Science and Technology (Guangzhou), Nansha, Guangzhou, Guangdong 511400, China

²Center for Theoretical Interdisciplinary Sciences, Wenzhou Institute, University of Chinese Academy of Sciences, Wenzhou, Zhejiang 325001, China

³Department of Chemistry and Physics, State University of New York at Stony Brook, Stony Brook, New York 11794, USA

(Received 21 September 2021; accepted 8 June 2022; published 4 August 2022)

We developed a nonequilibrium model to study chromosome structural reorganizations within a simplified cell developmental system. From the chromosome structural perspective, we predicted that the neural progenitor cell is on the neural developmental path and very close to the transdifferentiation path from the fibroblast to the neuron cell. We identified an early bifurcation of stem cell differentiation processes and the cell-of-origin-specific reprogramming pathways. Our theoretical results are in good agreement with available experimental evidence, promoting future applications of our approach.

DOI: 10.1103/PhysRevLett.129.068102

Cell-fate decision-making processes, which generate new cell states, are governed by an underlying gene regulation network [1]. The processes generally include the differentiation of the stem cell to the differentiated cell, the reprogramming as the reverse process of differentiation [2,3], and the transdifferentiation, which occurs directly between two differentiated cell types without going through the stem cell [4]. As the scaffold for gene expression, the 3D genome structure often undergoes large-scale changes to accommodate the new cell fate after the cell-state transition [5,6]. To understand the mechanisms of the differentiation, reprogramming, and transdifferentiation, it is crucial to reveal the genome structural reorganizations during the state-transition processes.

The task is challenging as it relies on the determination of the genome structure at both spatial and temporal scales with high resolution, simultaneously. During the last decade, our understanding of the 3D genome architecture has been tremendously increased by the Hi-C technique [7,8]. The measurement is in the form of a heat map, which describes the contact frequency formed by the two chromosomal loci across the genome. However, the Hi-C experiment is often performed at one stable cell state; thus it is impossible to study the chromosome structural dynamics when the cell state changes.

In light of the dynamical nature of the chromosomes, the 4D Nucleome methods, such as the time-course Hi-C technique, were recently developed to study the structural dynamics of chromosomes within various timescales [9,10]. Noteworthy, due to the sophisticated experimental procedures and high cost, the time-course Hi-C experiment can only be undertaken at a limited number of discrete time points. In addition, given the fact that the cellular dynamics at the

single-cell level are highly stochastic [11,12], the time-course data inevitably contain the temporal heterogeneity that further hinders our understanding of the intermediate states [13].

Here, we developed a theoretical and computational framework, which has great potential for studying the chromosome structural reorganizations at long temporal scales covering the cell-state transitions. The approach, referred to as the landscape-switching model, is described in the following (Fig. 1).

First, the Hi-C data-driven molecular dynamics (MD) simulations of the chromosome dynamics in one cell state

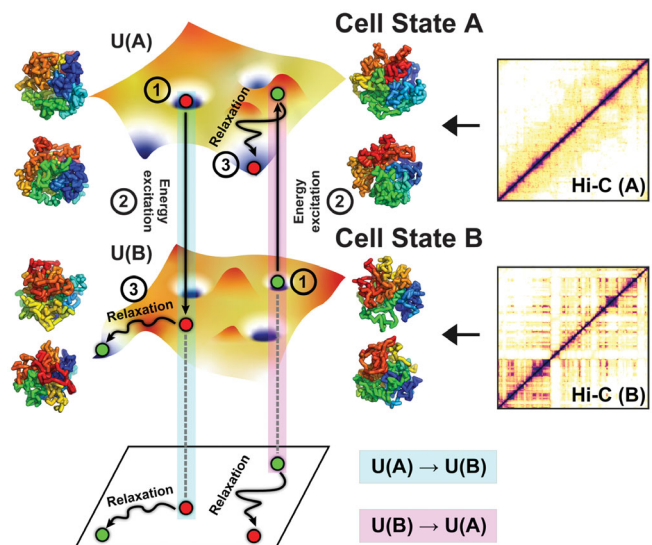


FIG. 1. An illustrative landscape-switching model for chromosome structural reorganizations during the cell-state transition processes.

are conducted. In MD simulations, the chromosome is represented by a beads-on-a-string model, where each bead mimics a segment of a DNA molecule on the genome. The energy function U contains two terms, which are the generic polymer potential V_{polymer} and the linear sum form of contact potential requested by the maximum entropy principle [14,15]: $U = V_{\text{polymer}} + \sum_{i,j} \alpha_{i,j} P_{i,j}$. $P_{i,j}$ is the contact probability formed by beads i and j . The parameters $\{\alpha_{i,j}\}$ are determined to generate a chromosome ensemble that reproduces the Hi-C data by maximizing the Shannon entropy $\mathbb{S}[\rho|\rho_0] = - \int d\mathbf{r} \rho(\mathbf{r}) \ln[\rho(\mathbf{r})/\rho_0(\mathbf{r})]$ on the distribution $\rho(\mathbf{r})$ under U relative to a given prior distribution $\rho_0(\mathbf{r})$ under V_{polymer} [16,17].

It is noteworthy that the model makes no assumptions about the nature of the molecular interactions; thus it does not describe the molecular events during the process of spatial chromosome organization. However, the data-driven strategy applied at the coarse-grained level can determine the physical interactions between the loci in organizing the chromosome structures without *a priori* knowledge about the details of the involving molecular processes, which are still largely unknown [18]. The resulting heterogeneous monomer interactions are deemed to account for the effects of the epigenetics on constructing the chromosome structural ensemble [19,20]. Furthermore, the potential U can be regarded as the effective landscape [21,22], which governs both the structural and dynamical properties of the chromosome within one cell state [23,24].

The chromosome is simulated under the potential $U(A)$ (A stands for the cell state A). Then the cell-state transition is triggered by an instantaneous energy excitation that switches the system from the cell state A into the state B via the landscape-switching implementation:

$$U(A) \xrightarrow{\text{switching}} U(B). \quad (1)$$

This implementation, which is in the form of an energy pump, breaks the detailed balance and drives the system out of equilibrium [25]. Finally, the chromosome is simulated under the potential $U(B)$, and the relaxation trajectories on $U(B)$ are collected to represent the cell-state transition process (Fig. 1, details in Supplemental Material [26]).

From the physical perspective, the landscape-switching model leads to a slow nonadiabatic nonequilibrium process. In a nonadiabatic nonequilibrium regime, the waiting time for interlandscape switching is longer than the timescales for intralandscape motion [63–65]. It has been well recognized that the cell-fate decision-making processes are supported by numerous sources of energy supplies, resulting in highly nonequilibrium dynamics. The processes, which do not occur spontaneously, are often slow and energy dependent, exhibiting slow nonadiabatic nonequilibrium dynamics [66]. From a biological perspective, the landscape-switching model leads to a process associated with switching of the

epigenetic modifications between two cell states. The cell developmental process has been found to be multistable, acting as a switch between different gene expression states that represent the stable cell states [67–71]. In addition, although the epigenetic modifications in individual loci can be quick and frequent, the switching of the cell states can only be realized by the cooperative changes of the histone states at a global scale [72,73]. These features support the approximate treatment of a cell-state transition as a bistable switch process.

Since Hi-C data are often measured by massive cells at the interphase, the landscape-switching model naturally leads to dynamical changes of the chromosome structural ensembles in the interphase during the cell-state transitions. In reality, cells often undergo multiple cell cycles to accomplish the cell-state transitions. The mitotic chromosome exhibits a highly condensed, uniformly cylinderlike structure, regardless of the cell type [74], and recovers to the specific cell-type-dependent form in the interphase after mitosis [12,75]. In this regard, it is a reasonable assumption that the chromosome condensation and decondensation during the cell cycle is nonspecific, based on the fact that the chromosome structure in the interphase upon the entry into mitosis can be fully reconstructed after the cell cycle. Thus, the chromosome structural dynamics during the cell-state transitions are a combination of the nonspecific cell-cycle-dependent condensation and decondensation and the specific cell-fate-dependent reorganizations, which likely occur only in the interphase [76]. Given the fact that cells spend most of the time residing in the interphase during the cell cycle, while the cell cycle has a much faster timescale than cell development, the fast dynamics of the cyclic nonspecific chromosome condensation and decondensation can be averaged out [77], rendering a focus on the slow dynamics occurring in the interphase. This implementation eventually leads to a simplified picture of chromosome structural reorganizations at the interphase of the cells during the cell-state transition processes, in line with the landscape-switching model (Fig. S1, details in the Supplemental Material [26]).

The landscape-switching model provided an effective way to simulate the chromosome structural reorganizations during the transitions among the pluripotent embryonic stem cell (ESC), the terminally differentiated fibroblast (Fibro), and the neuron (Neuron) cells. Our results showed that the chromosome can readily reach the structural ensemble at the new cell states by gradually adapting the contact probability map during simulations, which represent the cell-state switching processes [Fig. 2(a)]. To see whether the model is capable of correctly describing the chromosome structural changes, we then compared the chromosome structures from the simulations with the ones from the *in vivo* transitions, where the Hi-C data are available. In this regard, we focused on the neural progenitor cells (NPCs), which give rise to the Neuron cells upon differentiation. The chromosome during the neural

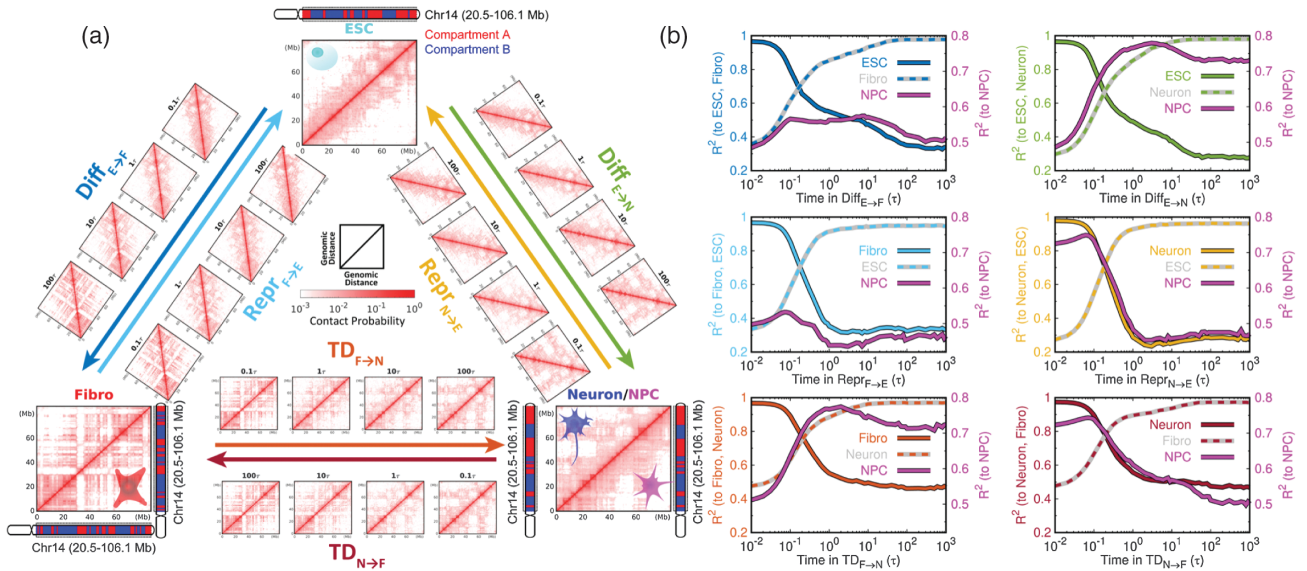


FIG. 2. Chromosome structural reorganizations during differentiation, reprogramming, and transdifferentiation. (a) The chromosome contact probability evolving along with time during the cell-state transitions. The contact maps of the ESC, NPC, Fibro, and Neuron cells are derived from the experimental Hi-C data. The contact maps at $t = 0.1\tau$, τ , 10τ , and 100τ of each transition are calculated, where τ is the unit of MD time. The ideograms of the chromosome segment used in our study (chr14: 20.5–106.1 Mb) are annotated by the compartment status at the corresponding cell state. The contact map is at the 100-kb resolution. (b) The correlation of the distance-corrected contact probability map during the transition with the ones at the initial (solid line) and final (dashed line) states of the transition, as well as the NPC (purple line) [78]. The correlation is indicated by the coefficient of determination R^2 .

differentiation from the ESC should adopt the structures at the NPCs and be structurally distinct from the ones on the developmental path of the Fibro cell.

For the ESC differentiation to the Fibro cell (Diff_{E→F}), we observed that the correlation R^2 of the simulated contact map with the experimental ones of the ESC and Fibro cell monotonically decreases and increases during the differentiation, respectively [Figs. 2(b) and S2 in the Supplemental Material [26]]. It characterizes and quantifies a cell developmental process, in which the chromosome gradually deforms the structures in the ESC and forms the structures in the differentiated cell. Interestingly, the correlation of the contact probabilities during the simulations with the Hi-C data of the NPC remains relatively weak, indicating that the chromosome does not adopt the structures in the NPC.

We found that R^2 of the simulated contact probabilities with the ones of the NPC and Neuron cell increases significantly during the ESC differentiation to the Neuron cell (Diff_{E→N}). Due to the highly correlated Hi-C data in the NPC and Neuron cell (Fig. S3 in the Supplemental Material [26]), the differentiation of the ESC to the Neuron cell not only increases the correlation of the contact map to the one at the Neuron cell, but also naturally increases the correlation to the NPC. However, we found that the initial increase of R^2 with the NPC during transition is followed by a decrease, in contrast to the monotonic increase of R^2 with the Neuron cell. The nonmonotonic profile of R^2 suggests that the transition initially approaches the NPC in terms of forming the

structures in the NPC, characterized by the highly correlated contact maps (Fig. S4 in the Supplemental Material [26]). The transition is then followed by proceeding to the Neuron cell through deformation of the structures in the NPC and formation of the structures in the Neuron cell, indicated by a decrease of the correlation in contact maps.

During reprogramming, the trajectories of R^2 do not exhibit to follow the reverse of those for the differentiation. The result indicates that reprogramming does not necessarily use the reversal of the developmental path, in line with the observations by previous experiments [79–81]. In addition, the slight increases after the significant decreases in R^2 with respect to the NPC and the initial cell states at the late stages of both reprogramming processes were observed. The finding is reminiscent of a recent experiment, where Cacchiarelli *et al.* characterized a nonmonotonic reprogramming trend in terms of the transcriptional activities and epigenomic profiles [82]. For the transdifferentiation between the Fibro and Neuron cells, we found the nonmonotonic R^2 profile for the transition from the Fibro to Neuron cells (TD_{F→N}), similar to the observation in the Diff_{E→N} transition. This suggests that the chromosome can adopt the structures in the NPC during the neural transdifferentiation. Our result is in line with the recent experimental finding that an NPC-like cell state was observed during the direct reprogramming of the Fibro to Neuron cells based on the single-cell transcriptomics data [83].

The 3D architectures of chromosomes are hierarchically organized from the mega-base-sized topologically

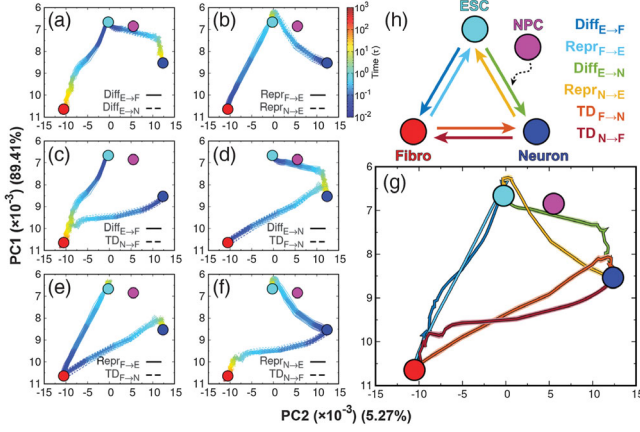


FIG. 3. Quantified chromosome structural reorganization pathways during differentiation, reprogramming, and transdifferentiation from the TADs perspective. The quantified pathways are shown in the PCA plots of the insulation score profiles projected at the first two PCs for (a) differentiation, (b) reprogramming, (c) conversion to the Fibro cell, (d) conversion to the Neuron cell, (e) deformation from the Fibro cell, and (f) deformation from the Neuron cell. The averaged pathways are collected and shown in (g). The shadow regions indicate the error bars of the averaged pathways from the bootstrapping analysis. The scheme illustrating the six cell-state transitions is shown in (h).

associating domains (TADs) [84–86] to the long-range phase-segregated compartments, which span multiple megabases of DNA [7]. The chromosomal loci within one TAD exhibit strong interactions, while the interactions between the loci across the TAD are highly reduced. We used the insulation score introduced by Crane *et al.* to describe the TAD structural formation (Fig. S5 in the Supplemental Material [26]) [87]. The insulation score, which is calculated from the contact map, has been widely used to identify the TAD boundaries and further the TAD formation. A lower (higher) insulation score corresponds to a stronger (weaker) local insulation tendency to form the TAD boundary. We collected all the insulation score profiles along the simulation trajectories and generated the principal component analysis (PCA) plots (details in Supplemental Material [26]). The insulation score profile at each time point was projected as one dot onto the first two principal components (PCs), and the distances between the dots on the plots indicate the differences between the insulation score profile at different time points (Fig. 3).

From the TAD structural perspective, we found that the NPC is on the path from the ESC differentiation to the Neuron cell ($\text{Diff}_{E \rightarrow N}$) [Fig. 3(a)]. In contrast, the differentiation pathways of the ESC to Fibro cells ($\text{Diff}_{E \rightarrow F}$) do not go through the NPC, as these two differentiation pathways bifurcate at the very early stage from the ESC. Interestingly, the NPC is not located on the pathways of reprogramming from the Neuron cell to the ESC, though the distance between the NPC and paths is not very significant [Fig. 3(b)]. These two reprogramming pathways

from different differentiated cells ($\text{Repr}_{F \rightarrow E}$ and $\text{Repr}_{N \rightarrow E}$) merge at the late stages very close to the ESC.

We further compared the processes of forming the differentiated cell through the ESC (via differentiation) and the other differentiated cell (via transdifferentiation) [Figs. 3(c) and 3(d)]. We found that the pathways toward the same destination only overlap at the very late stages, suggesting that the initial state of the transition defines the specificity of the pathways. It is noteworthy that the NPC is not located on the pathways of the Fibro to Neuron transition ($\text{TD}_{F \rightarrow N}$). This is consistent with the experimental evidence that the NPC-like intermediate state during the transdifferentiation from the Fibro to Neuron cells shows a deviation of gene expression patterns from the canonical NPC [83]. By examining the pathways of deforming Fibro and Neuron [Figs. 3(e) and 3(f)], we found that these two pathways bifurcate at the very early stages.

By collecting all the trajectories, we calculated the averaged pathways of the cell-fate decision-making processes for this simple three-cell system. Two features can be captured. First, there is irreversibility for the two processes in the opposite directions between any pair of these three cell states [Fig. 3(g)]. The irreversibility reflects the non-equilibrium essence of the cell-fate decision-making processes. Second, our results at the TAD structural level predict that the NPC is formed during the ESC differentiation to the Neuron cell [Fig. 3(h)].

We further performed a similar PCA on the simulation trajectories of the enhanced contact probability matrix $P_{\text{obs}}/P_{\text{exp}}$, where P_{obs} and P_{exp} are the observed and expected contact probability at 1-Mb resolution (details in Supplemental Material [26]). The matrix $P_{\text{obs}}/P_{\text{exp}}$ provides the information of the compartment formation at the long range (Fig. S6 in the Supplemental Material [26]) [7,88]. Similar to the observations of TADs on the PCA plots, we found that the differentiation pathways toward different somatic cells from the ESC bifurcate at the early stages [Fig. 4(a)] and differentiated cell reprogramming pathways

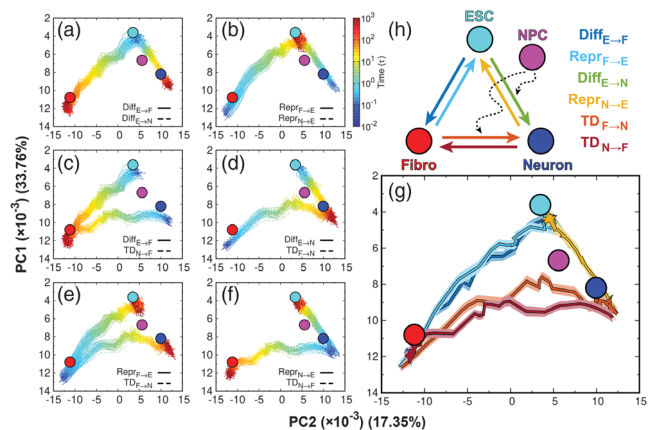


FIG. 4. The same as Fig. 3, but the PCA plots are done for contact probability $\log_2(P_{\text{obs}}/P_{\text{exp}})$.

merge at the late stages [Fig. 4(b)]. Previous experiments found that the somatic cell reprogramming exhibits cell-of-origin-specific 3D genome structures at the early stages of forming the pluripotent cells [89,90]. The convergence of the paths from different cells to the final states occurs only at the very late stages of reprogramming, where the massive changes in the chromosome structures have already been accomplished, resulting in the ESC-like states [89]. Our predictions on the quantified pathways are in very good agreement with these experimental observations. We also found that the NPC is very close to the neural differentiation ($\text{Diff}_{E \rightarrow N}$) [Fig. 4(a)] and transdifferentiation pathways ($\text{TD}_{F \rightarrow N}$) [Fig. 4(d)], but not the reverse transdifferentiation pathways [Fig. 4(c)]. The results suggest that the chromosome can adopt the structures at the NPC during the neural developmental and transdifferentiation processes [Fig. 4(h)], in line with the experimental characterization on the Fibro-to-Neuron transdifferentiation pathways [83]. The early bifurcation of the transition pathways from the same initial states was also observed at the level of $P_{\text{obs}}/P_{\text{exp}}$ [Figs. 4(e)–4(g)].

Because the detailed molecular nature of the interactions was not considered, our model does not explicitly capture the protein-mediated processes that drive the chromosome organization, such as the loop extrusion in TADs [91] and heterochromatin protein 1 involved phase separation in compartmentalizations [92]. In fact, the trajectories from our simulations describe the cell-state transition-triggered dynamical rearrangements of the chromosome structure ensembles, which are the eventual results from these molecular processes. In addition, our model focuses on the chromosome structural reorganizations at interphase during the cell-state transitions; thus it does not aim to fully capture the underlying dynamics of the processes. To seek the microscopic molecular-level mechanisms of chromosome structural dynamics in cell-state transitions, future improvements can be targeted by incorporating the promising mechanistic models into the landscape-switch approach [18] and explicitly taking into account the cell-cycle processes [93].

Our model combines the equilibrium and nonequilibrium approaches in one simple unified framework, which captures the nonadiabatic nonequilibrium phenotypic switching essence of the complex cell-state transition. Our finding enables an advanced understanding of the processes from the landscape perspective (Fig. S7 in the Supplemental Material [26]). The good agreement between the simulations and experiments promotes the model as a general approach that goes beyond the interpolation-based method (Figs. S8–S11, details in Supplemental Material [26]) [13,94].

*jin.d.wang@gmail.com

- [1] N. Moris, C. Pina, and A. M. Arias, *Nat. Rev. Genet.* **17**, 693 (2016).
 [2] K. Takahashi and S. Yamanaka, *Cell* **126**, 663 (2006).

- [3] K. Takahashi, K. Tanabe, M. Ohnuki, M. Narita, T. Ichisaka, K. Tomoda, and S. Yamanaka, *Cell* **131**, 861 (2007).
 [4] C. Jopling, S. Boue, and J. C. I. Belmonte, *Nat. Rev. Mol. Cell Biol.* **12**, 79 (2011).
 [5] H. Zheng and W. Xie, *Nat. Rev. Mol. Cell Biol.* **20**, 535 (2019).
 [6] A. M. Oudelaar and D. R. Higgs, *Nat. Rev. Genet.* **22**, 154 (2021).
 [7] E. Lieberman-Aiden, N. L. Van Berkum, L. Williams, M. Imakaev, T. Ragoczy, A. Telling, I. Amit, B. R. Lajoie, P. J. Sabo, M. O. Dorschner *et al.*, *Science* **326**, 289 (2009).
 [8] S. S. Rao, M. H. Huntley, N. C. Durand, E. K. Stamenova, I. D. Bochkov, J. T. Robinson, A. L. Sanborn, I. Machol, A. D. Omer, E. S. Lander, and E. L. Aiden, *Cell* **159**, 1665 (2014).
 [9] J. Dekker, A. S. Belmont, M. Guttman, V. O. Leshyk, J. T. Lis, S. Lomvardas, L. A. Mirny, C. C. O Shea, P. J. Park, B. Ren *et al.*, *Nature (London)* **549**, 219 (2017).
 [10] M. A. Marti-Renom, G. Almouzni, W. A. Bickmore, K. Bystrycky, G. Cavalli, P. Fraser, S. M. Gasser, L. Giorgetti, E. Heard, M. Nicodemi *et al.*, *Nat. Genet.* **50**, 1352 (2018).
 [11] T. Nagano, Y. Lubling, T. J. Stevens, S. Schoenfelder, E. Yaffe, W. Dean, E. D. Laue, A. Tanay, and P. Fraser, *Nature (London)* **502**, 59 (2013).
 [12] T. Nagano, Y. Lubling, C. Várnai, C. Dudley, W. Leung, Y. Baran, N. M. Cohen, S. Wingett, P. Fraser, and A. Tanay, *Nature (London)* **547**, 61 (2017).
 [13] K. Abramo, A.-L. Valton, S. V. Venev, H. Ozadam, A. N. Fox, and J. Dekker, *Nat. Cell Biol.* **21**, 1393 (2019).
 [14] A. Cesari, S. Reißer, and G. Bussi, *Computation* **6**, 15 (2018).
 [15] X. Lin, Y. Qi, A. P. Latham, and B. Zhang, *J. Chem. Phys.* **155**, 010901 (2021).
 [16] B. Zhang and P. G. Wolynes, *Proc. Natl. Acad. Sci. U.S.A.* **112**, 6062 (2015).
 [17] B. Zhang and P. G. Wolynes, *Phys. Rev. Lett.* **116**, 248101 (2016).
 [18] C. A. Brackey, D. Marenduzzo, and N. Gilbert, *Nat. Methods* **17**, 767 (2020).
 [19] M. Di Pierro, B. Zhang, E. L. Aiden, P. G. Wolynes, and J. N. Onuchic, *Proc. Natl. Acad. Sci. U.S.A.* **113**, 12168 (2016).
 [20] M. Di Pierro, R. R. Cheng, E. L. Aiden, P. G. Wolynes, and J. N. Onuchic, *Proc. Natl. Acad. Sci. U.S.A.* **114**, 12126 (2017).
 [21] S. Wang and P. G. Wolynes, *J. Chem. Phys.* **135**, 051101 (2011).
 [22] S. Wang and P. Wolynes, *J. Chem. Phys.* **136**, 145102 (2012).
 [23] L. Liu, G. Shi, D. Thirumalai, and C. Hyeon, *PLoS Comput. Biol.* **14**, e1006617 (2018).
 [24] M. Di Pierro, D. A. Potoyan, P. G. Wolynes, and J. N. Onuchic, *Proc. Natl. Acad. Sci. U.S.A.* **115**, 7753 (2018).
 [25] X. Fang, K. Kruse, T. Lu, and J. Wang, *Rev. Mod. Phys.* **91**, 045004 (2019).
 [26] See Supplemental Material at <http://link.aps.org/supplemental/10.1103/PhysRevLett.129.068102> for further details of methods and results, which includes Refs. [27–62].

- [27] P. Rajarajan, T. Borrmann, W. Liao, N. Schrode, E. Flaherty, C. Casiño, S. Powell, C. Yashaswini, E. A. LaMarca, B. Kassim *et al.*, *Science* **362**, eaat4311 (2018).
- [28] N. Servant, N. Varoquaux, B. R. Lajoie, E. Viara, C.-J. Chen, J.-P. Vert, E. Heard, J. Dekker, and E. Barillot, *Genome Biol.* **16**, 259 (2015).
- [29] M. Imakaev, G. Fudenberg, R. P. McCord, N. Naumova, A. Goloborodko, B. R. Lajoie, J. Dekker, and L. A. Mirny, *Nat. Methods* **9**, 999 (2012).
- [30] K. Kremer and G. S. Grest, *J. Chem. Phys.* **92**, 5057 (1990).
- [31] H. R. Warner Jr, *Ind. Eng. Chem. Fundam.* **11**, 379 (1972).
- [32] N. Tokuda, T. P. Terada, and M. Sasai, *Biophys. J.* **102**, 296 (2012).
- [33] J. C. Wang, *Biochim. Biophys. Acta* **909**, 1 (1987).
- [34] J. R. Swedlow, J. W. Sedat, and D. A. Agard, *Cell* **73**, 97 (1993).
- [35] L. Poljak and E. Käs, *Trends Cell Biol.* **5**, 348 (1995).
- [36] J. H. Lee and J. M. Berger, *Genes* **10**, 859 (2019).
- [37] A. Rosa and R. Everaers, *PLoS Comput. Biol.* **4**, e1000153 (2008).
- [38] X. Chu and J. Wang, *Adv. Sci.* **7**, 2001572 (2020).
- [39] V. Dileep, K. A. Wilson, C. Marchal, X. Lyu, P. A. Zhao, B. Li, A. Poulet, D. A. Bartlett, J. C. Rivera-Mulia, Z. S. Qin *et al.*, *Stem Cell Rep.* **13**, 193 (2019).
- [40] K. N. Klein, P. A. Zhao, X. Lyu, T. Sasaki, D. A. Bartlett, A. M. Singh, I. Tasan, M. Zhang, L. P. Watts, S.-i. Hiraga *et al.*, *Science* **372**, 371 (2021).
- [41] G. Fudenberg and L. A. Mirny, *Curr. Opin. Genet. Dev.* **22**, 115 (2012).
- [42] T. Yang, F. Zhang, G. G. Yardımcı, F. Song, R. C. Hardison, W. S. Noble, F. Yue, and Q. Li, *Genome Res.* **27**, 1939 (2017).
- [43] Q. Sun, A. Perez-Rathke, D. M. Czajkowsky, Z. Shao, and J. Liang, *Nat. Commun.* **12**, 1 (2021).
- [44] M. G. Guenther, G. M. Frampton, F. Soldner, D. Hockemeyer, M. Mitalipova, R. Jaenisch, and R. A. Young, *Cell Stem Cell* **7**, 249 (2010).
- [45] J. Choi, S. Lee, W. Mallard, K. Clement, G. M. Tagliazucchi, H. Lim, I. Y. Choi, F. Ferrari, A. M. Tsankov, R. Pop *et al.*, *Nat. Biotechnol.* **33**, 1173 (2015).
- [46] J. Bilic and J. C. I. Belmonte, *Stem Cells* **30**, 33 (2012).
- [47] B. Aydin and E. O. Mazzoni, *Annu. Rev. Cell Dev. Biol.* **35**, 433 (2019).
- [48] J. A. Briggs, V. C. Li, S. Lee, C. J. Woolf, A. Klein, and M. W. Kirschner, *eLife* **6**, e26945 (2017).
- [49] C. H. Waddington, *The Strategy of the Genes* (Allen and Unwin, London, 1957).
- [50] J. Wang, K. Zhang, L. Xu, and E. Wang, *Proc. Natl. Acad. Sci. U.S.A.* **108**, 8257 (2011).
- [51] J. Wang, L. Xu, and E. Wang, *Proc. Natl. Acad. Sci. U.S.A.* **105**, 12271 (2008).
- [52] B. Hess, C. Kutzner, D. Van Der Spoel, and E. Lindahl, *J. Chem. Theory Comput.* **4**, 435 (2008).
- [53] G. A. Tribello, M. Bonomi, D. Branduardi, C. Camilloni, and G. Bussi, *Comput. Phys. Commun.* **185**, 604 (2014).
- [54] J. Ostashevsky and C. Lange, *J. Biomol. Struct. Dyn.* **11**, 813 (1994).
- [55] S. Shinkai, T. Nozaki, K. Maeshima, and Y. Togashi, *PLoS Comput. Biol.* **12**, e1005136 (2016).
- [56] X. Chu and J. Wang, *JACS Au* **2**, 116 (2021).
- [57] X. Chu and J. Wang, *PLoS Comput. Biol.* **17**, e1009596 (2021).
- [58] A. L. Sanborn, S. S. Rao, S.-C. Huang, N. C. Durand, M. H. Huntley, A. I. Jewett, I. D. Bochkov, D. Chinnappan, A. Cutkosky, J. Li *et al.*, *Proc. Natl. Acad. Sci. U.S.A.* **112**, E6456 (2015).
- [59] F. Uhlmann, *Nat. Rev. Mol. Cell Biol.* **17**, 399 (2016).
- [60] M. Ganji, I. A. Shaltiel, S. Bisht, E. Kim, A. Kalichava, C. H. Haering, and C. Dekker, *Science* **360**, 102 (2018).
- [61] A. G. Larson, D. Elnatan, M. M. Keenen, M. J. Trnka, J. B. Johnston, A. L. Burlingame, D. A. Agard, S. Redding, and G. J. Narlikar, *Nature (London)* **547**, 236 (2017).
- [62] J. Nuebler, G. Fudenberg, M. Imakaev, N. Abdennur, and L. A. Mirny, *Proc. Natl. Acad. Sci. U.S.A.* **115**, E6697 (2018).
- [63] J. N. Onuchic and P. G. Wolynes, *J. Phys. Chem.* **92**, 6495 (1988).
- [64] K. Zhang, M. Sasai, and J. Wang, *Proc. Natl. Acad. Sci. U.S.A.* **110**, 14930 (2013).
- [65] J. Wang, *Adv. Phys.* **64**, 1 (2015).
- [66] X. Chu and J. Wang, *Appl. Phys. Rev.* **7**, 031403 (2020).
- [67] J. E. Ferrell and E. M. Machleder, *Science* **280**, 895 (1998).
- [68] W. Xiong and J. E. Ferrell, *Nature (London)* **426**, 460 (2003).
- [69] S. Huang, G. Eichler, Y. Bar-Yam, and D. E. Ingber, *Phys. Rev. Lett.* **94**, 128701 (2005).
- [70] H. H. Chang, M. Hemberg, M. Barahona, D. E. Ingber, and S. Huang, *Nature (London)* **453**, 544 (2008).
- [71] X. Fang, Q. Liu, C. Bohrer, Z. Hensel, W. Han, J. Wang, and J. Xiao, *Nat. Commun.* **9**, 1 (2018).
- [72] M. Sasai, Y. Kawabata, K. Makishi, K. Itoh, and T. P. Terada, *PLoS Comput. Biol.* **9**, e1003380 (2013).
- [73] S. Ashwin and M. Sasai, *Sci. Rep.* **5**, 16746 (2015).
- [74] N. Naumova, M. Imakaev, G. Fudenberg, Y. Zhan, B. R. Lajoie, L. A. Mirny, and J. Dekker, *Science* **342**, 948 (2013).
- [75] J. H. Gibcus, K. Samejima, A. Goloborodko, I. Samejima, N. Naumova, J. Nuebler, M. T. Kanemaki, L. Xie, J. R. Paulson, W. C. Earnshaw *et al.*, *Science* **359**, eaa06135 (2018).
- [76] W. F. Chan, H. D. Coughlan, J. H. Zhou, C. R. Keenan, N. G. Bediaga, P. D. Hodgkin, G. K. Smyth, T. M. Johanson, and R. S. Allan, *Nat. Commun.* **12**, 1 (2021).
- [77] A. Krakovsky, *AIP Adv.* **8**, 085301 (2018).
- [78] S. Bianco, D. G. Lupiáñez, A. M. Chiariello, C. Annunziatella, K. Kraft, R. Schöpflin, L. Wittler, G. Andrey, M. Vingron, A. Pombo *et al.*, *Nat. Genet.* **50**, 662 (2018).
- [79] K. Takahashi and S. Yamanaka, *Development* **142**, 3274 (2015).
- [80] R. Stadhouders, E. Vidal, F. Serra, B. Di Stefano, F. Le Dily, J. Quilez, A. Gomez, S. Collombet, C. Berenguer, Y. Cuartero *et al.*, *Nat. Genet.* **50**, 238 (2018).
- [81] H. Miura, S. Takahashi, R. Poonperm, A. Tanigawa, S.-i. Takebayashi, and I. Hiratani, *Nat. Genet.* **51**, 1356 (2019).
- [82] D. Cacchiarelli, C. Trapnell, M. J. Ziller, M. Soumillon, M. Cesana, R. Karnik, J. Donaghey, Z. D. Smith, S. Ratanasirintrao, X. Zhang *et al.*, *Cell* **162**, 412 (2015).
- [83] B. Treutlein, Q. Y. Lee, J. G. Camp, M. Mall, W. Koh, S. A. M. Shariati, S. Sim, N. F. Neff, J. M. Skotheim, M. Wernig, and S. R. Quake, *Nature (London)* **534**, 391 (2016).

- [84] J. R. Dixon, S. Selvaraj, F. Yue, A. Kim, Y. Li, Y. Shen, M. Hu, J. S. Liu, and B. Ren, *Nature (London)* **485**, 376 (2012).
- [85] E. P. Nora, B. R. Lajoie, E. G. Schulz, L. Giorgetti, I. Okamoto, N. Servant, T. Piolot, N. L. van Berkum, J. Meisig, J. Sedat *et al.*, *Nature (London)* **485**, 381 (2012).
- [86] T. Sexton, E. Yaffe, E. Kenigsberg, F. Bantignies, B. Leblanc, M. Hoichman, H. Parrinello, A. Tanay, and G. Cavalli, *Cell* **148**, 458 (2012).
- [87] E. Crane, Q. Bian, R. P. McCord, B. R. Lajoie, B. S. Wheeler, E. J. Ralston, S. Uzawa, J. Dekker, and B. J. Meyer, *Nature (London)* **523**, 240 (2015).
- [88] J. R. Dixon, I. Jung, S. Selvaraj, Y. Shen, J. E. Antosiewicz-Bourget, A. Y. Lee, Z. Ye, A. Kim, N. Rajagopal, W. Xie *et al.*, *Nature (London)* **518**, 331 (2015).
- [89] P. H. L. Krijger, B. Di Stefano, E. de Wit, F. Limone, C. Van Oevelen, W. De Laat, and T. Graf, *Cell Stem Cell* **18**, 597 (2016).
- [90] C. M. Nefzger, F. J. Rossello, J. Chen, X. Liu, A. S. Knaupp, J. Firas, J. M. Paynter, J. Pflueger, S. Buckberry, S. M. Lim *et al.*, *Cell Rep.* **21**, 2649 (2017).
- [91] G. Fudenberg, M. Imakaev, C. Lu, A. Goloborodko, N. Abdennur, and L. A. Mirny, *Cell Rep.* **15**, 2038 (2016).
- [92] A. R. Strom, A. V. Emelyanov, M. Mir, D. V. Fyodorov, X. Darzacq, and G. H. Karpen, *Nature (London)* **547**, 241 (2017).
- [93] H. Miura and I. Hiratani, *Curr. Opin. Genet. Dev.* **73**, 101898 (2022).
- [94] M. Highsmith and J. Cheng, *Int. J. Mol. Sci.* **22**, 9785 (2021).